Growth and Characterization of Sb_2Se_3 Single Crystals for Fundamental Studies

Theodore D. C. Hobson*, Oliver S. Hutter, Max Birkett, Tim D. Veal and Ken Durose

Stephenson Institute for Renewable Energy, University of Liverpool, Chadwick Building, Peach Street, Liverpool L69 7ZF UK

*thobson@liverpool.ac.uk

***Abstract* — Three methods of growing bulk crystalline samples of Sb_2Se_3 to provide material for basic studies have been investigated and preliminary characterization is reported. These growth methods were: a) melt-growth, similar to vertical Bridgman, b) dynamic vapor transport over a temperature gradient (Piper-Polich method) and c) a static vapor method in which the source material is transported in nearly iso-thermal conditions. The melt-growth method produced the largest single crystals (up to 4 mm diameter), while the vapor methods both yielded polycrystalline boules with mm-sized grains. Powder XRD confirmed the boules to comprise orthorhombic Sb_2Se_3, having lattice parameters *a* = 11.7808 Å, *b* = 3.9767 Å and *c* = 11.6311 Å. Cleavage facets were parallel to (100). Raman peaks at 191 (A_g) and 211 cm^{-1} were excited anisotropically. FTIR reflectance features showed some sensitivity to s- and p-polarization.**

***Index Terms* — antimony selenide, crystal growth, Raman spectroscopy, single crystal, X-ray diffraction.**

I. Introduction

Antimony selenide (Sb_2Se_3) offers an attractive alternative to established thin-film photovoltaic (PV) technologies such as CdTe and CIGS, due to its relatively cheap and plentiful constituents and low-toxicity [1]. Its band gap , 1.1-1.3eV [1], is within the optimum range for PV devices, and presently the highest performing devices have efficiencies of 6.5% [2]. Recent studies using closed-space sublimation as a fabrication technique give similar efficiencies [3], [4]. Despite these impressive steps forward there has been relatively little fundamental characterization of Sb_2Se_3 to date.

The low symmetry of the crystal structure of Sb_2Se_3 arises since lattice distortion stabilizes a $5s^2$ lone pair in an antibonding position, and this systematically blocks a bonding direction. Hence while the ribbons in the Sb_2Se_3 lattice are covalently bonded, adjacent ribbons are connected by van der Waals forces. It has therefore been suggested that grain boundaries in Sb_2Se_3 may be engineered to be van der Waals bonded, and that the Shockley Reed Hall recombination associated with dangling-covalent bonds may be avoided [5]. Moreover conduction is expected to be higher along the ribbon axis [5]. Additionally, density-functional theory calculations suggest that Sb_2Se_3 will display anisotropic optical absorption [6] which has important implications for PV device architectures. Since these phenomena have not been fully investigated by experiment, there is a requirement to grow the necessary bulk single- and large-grained crystals – and it is the crystal growth that is the subject of this work.

Sb_2Se_3 is orthorhombic and its space group (number 62) is variously reported as *Pbnm* [7] or *Pnma* [8]. These differ only in the order of the Miller indices used e.g. the cleavage plane is (100) in the *Pnma* convention used throughout this work rather than (010) in the *Pbnm* convention.

Previously, large single crystals of Sb_2Se_3 have been produced using the Bridgman growth technique, but without the intention to measure properties relevant to photovoltaics [9].

In this work we demonstrate the production of large single-crystals of Sb_2Se_3 using a simplified form of Bridgman growth in a single zone furnace, as well as large-grained polycrystalline boules through static and dynamic (Piper-Polich) vapor transport. The largest single crystals were produced from the vertical-gradient freeze technique at around 3 cm long and with a diameter of 4 mm.

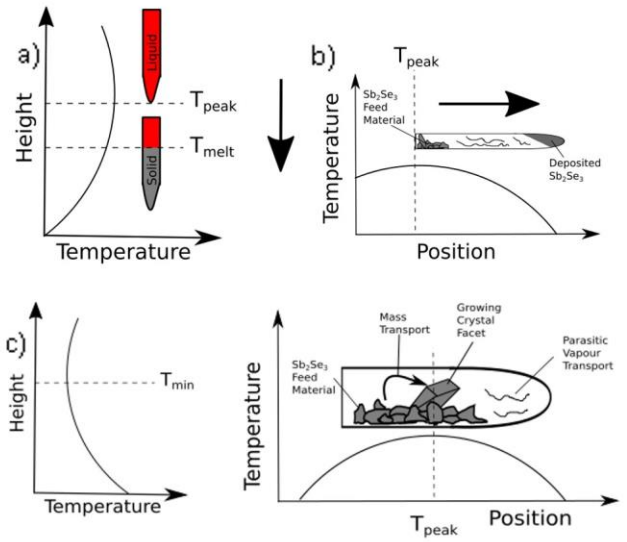

Fig. 1. Diagrams illustrating a) melt-growth (vertical Bridgman) – the bold arrow shows the direction of the ampoule's movement, b) Piper-Polich 'dynamic vapor transport' in a static ampoule - bold arrow showing direction of vapor transport and c) the 'static vapor growth' method, showing (left) vertical temperature profile of the tube furnace and (right) the process of mass transport and the horizontal temperature profile of the furnace.

II. Experimental Methods

For the melt-growth of single crystals, quartz tubes of 4mm internal diameter (ID) were charged with ~7g of Sb_2Se_3 powder (5N, Alfa Aesar), flushed with argon, evacuated to 10^{-5} mbar and sealed. The ampoules were placed in a single zone vertical furnace with the tip at the position of the peak temperature of 615°C (this temperature being just above the melting point of Sb_2Se_3 at 611°C [10], Fig. 1a). The ampoule was then lowered at a rate of 1.15 mm/hr through the furnace, the temperature gradient being around 6°C/cm, for 7 days. (This method differs from most vertical Bridgman implementations in that the temperature gradient in single zone furnace rather than an engineered temperature gradient was used). Unexpectedly, in addition to the boules formed from the melt, this method produced long, needle-like crystals from condensation of the vapor present in the ampoule.

For the 'static vapor growth' method, quartz tubes were charged with Sb_2Se_3 and sealed by the same method as for melt-growth. Ampoules were placed at the center of a single zone open-ended horizontal tube furnace at a peak temperature of 605°C i.e. just below the melting point of Sb_2Se_3 [10], to maximize vaporization while ensuring the grown crystals could fully solidify. This method was designed to exploit the vertical temperature gradient present in a horizontal tube furnace as shown in Fig. 1c. (This geometry has been described for the 'self-selecting vapor growth' (SSVG) process, but in this work a single zone furnace, rather than the three zone furnace required for ideal SSVG [11], was used). Small ampoules (4 mm ID, 8 cm length) with a large quantity of feed material (filling around half the ampoule) were chosen to restrict Piper-Polich-like mass transport during the 14-day growth process, and hence encouraging SSVG-like transport.

For the 'dynamic vapor growth', in contrast, Piper-Polich transport was encouraged by using tubes with a larger free-volume (10 mm ID and 7 cm length), placed such that a horizontal temperature gradient of around 15°C/cm existed between the charge and the tube-tip so as to drive transport, as shown in Fig. 1b. These samples were left until all of the material had transported, which took 10-14 days depending on the positioning of the ampoule in the furnace.

Grown samples were characterized as follows: scanning electron microscopy (SEM) was carried out on boules produced from static vapor growth using a JEOL-7001 FEGSEM electron microscope with an acceleration voltage of 5 kV. Optical microscopy was carried out using a Nikon Eclipse LV100 microscope at 5x magnification. Powder X-ray diffraction (XRD) was carried on all samples with a Rigaku Smartlab X-ray diffractometer in parallel beam geometry, with powders finely ground using a pestle and mortar. Single crystal XRD was carried out on the cleaved surface of the melt-grown crystals using the same equipment, also in parallel beam geometry. Unpolarized Raman spectroscopy was carried out on all samples using a Horiba Xplorer Plus Raman microscope with a laser wavelength of 532 nm. Cleavage facets were used for Raman characterization where available - otherwise samples were cut with a diamond saw, mechanically polished with 0.3µm alumina grit and chemically polished in 0.2 vol% Br-MeOH solution for 3 mins. Fourier transform infrared spectroscopy (FTIR) was carried out at room temperature on polished faces of samples produced from dynamic vapor growth using a Bruker Vertex 70v vacuum spectrometer with a mid-infrared silicon carbide globar light-source and DLaTGS detector.

III. Results

A. Appearance, Grain Structure and Cleavage

Photographs of a typical melt-grown crystal are shown in Fig. 2. The crystals were about 3 cm long, with the first 1.5 – 2 cm being polycrystalline. The single crystal part cleaved easily revealing bright shiny (100) cleavage facets (see XRD later).

The static vapor growth technique produced small polycrystalline boules at the bottom of the ampoule, having rough surfaces and grooves suggesting grain boundaries. Cleavage confirmed the polycrystallinity.

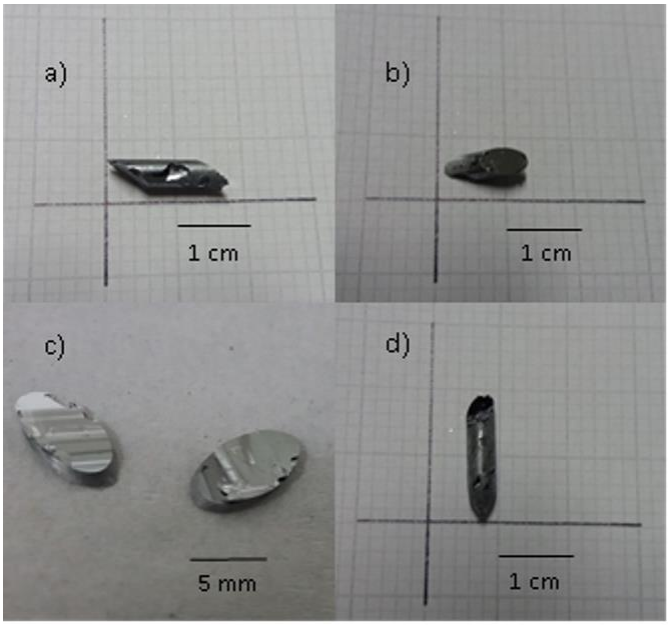

Fig. 2. Photographs of melt-grown Sb_2Se_3 crystals showing cleavage facets. The as-grown crystals were 4 mm in diameter and 3 cm long.

SEM carried out on pieces of crystal formed by static vapor growth showed both grain boundaries and cleavage planes as shown in Fig. 3a. The grain sizes ranged from 0.5 (Fig. 3a) to 2 mm (Fig 3c). Since the grain size of the feedstock was in the

range 1 – 5 μm, this confirms that the expected transport from the bottom of the source to the top (hence forming growing crystals on the top of the feedstock) had indeed taken place.

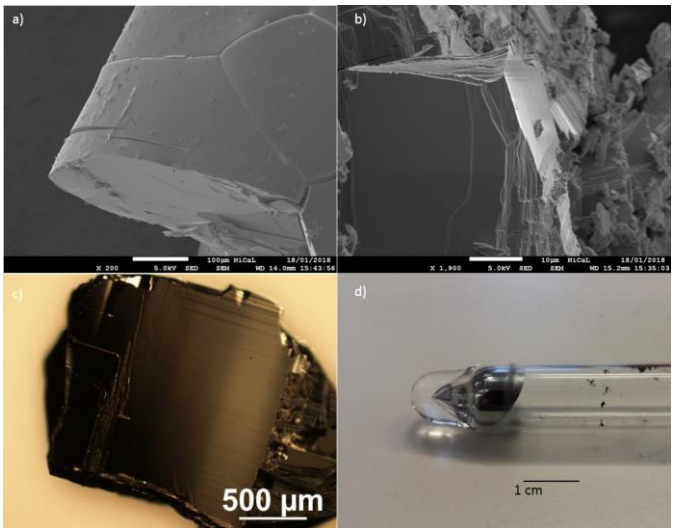

Fig. 3. a) Surface of static vapor-grown Sb_2Se_3 showing the grain boundaries, b) and (100) cleavage facets. c) Optical microscope image of the cleaved crystal face of static vapor-grown crystal. d) Polycrystalline Sb_2Se_3 ingot formed from dynamic vapor transport.

The dynamic vapor growth (Piper-Polich) technique produced a solid cone-shaped boule at the tube tip. While the whole boule diameter could not be cleaved cleanly, tapping the edges revealed crystal facets up to several mm in size. The grain sizes are therefore comparable to those grown by the static vapor method.

B. X-ray Diffraction

Fig. 4 shows a comparison of the powder XRD for Sb_2Se_3 feedstock and for a ground up sample of the dynamic vapor-grown crystal. There is a close match between the two, and Rietveld refinement confirmed the *Pnma* orthorhombic structure as expected both from experiment and density functional theory [8]. Similar results were also found for powderized melt-grown and static vapor-grown samples. Rietveld refinement yielded lattice parameters of a = 11.7802 Å, b = 3.9762 Å and c = 11.6302 Å from the former (χ^2 = 5.1) and a = 11.7808 Å, b = 3.9767 Å and c = 11.6311 Å (χ^2 = 2.38) from the latter. Clearly both melt- and vapor growth methods are capable of generating the required composition, and it may be assumed that vaporization is approximately congruent.

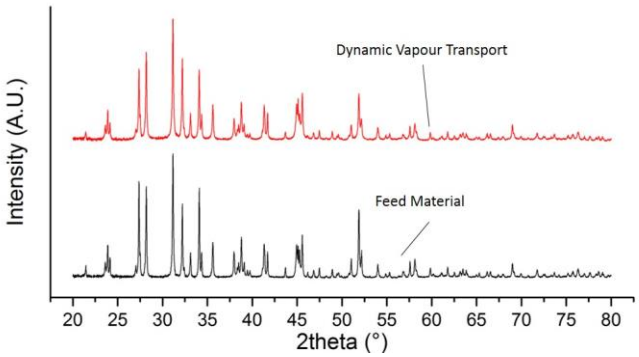

Fig. 4. Powder XRD θ - 2θ scan of polycrystalline feed material and the material crystallized from dynamic vapor transport after powderization confirming growth of Sb_2Sb_3.

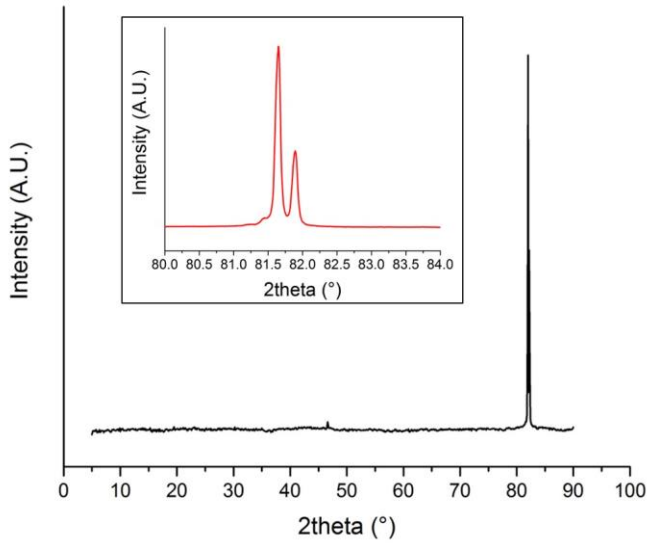

Fig. 5 θ-2θ XRD pattern of a cleaved melt-grown Sb_2Se_3 single crystal showing the (10 0 0) peak at ~82°, and its $K\alpha_1$ / $K\alpha_2$ doublet.

Fig. 5 shows a θ-2θ XRD pattern recorded from the cleavage facet of a melt-grown Sb_2Se_3 single crystal. The single strong peak at ~82° is resolved into K-α_1 and K-α_2 components at 81.65° and 81.89° as shown in the inset. These peaks correspond to the positions expected for the (10 0 0) reflection of Sb_2Se_3 based on the lattice parameter measured above. Since the θ-2θ method measures the interplanar spacing perpendicular to the sample's surface (in this case a cleavage facet), this measurement confirms the cleavage plane to be parallel to (100) as reported in the literature [12].

C. Raman Spectroscopy

Unpolarized Raman spectra were taken from faces of melt-grown single crystals cut both parallel to the growth direction and at 90° to it. The two sets of spectra, as shown in Fig. 6, both showed the characteristic peaks of Sb_2Se_3, at 191cm^{-1} and

211cm^{-1}, but having different relative intensities depending on the sample orientation. The 191cm^{-1} peak has been reported to correspond to the A_g mode [12] while further study may be needed to assign the 211cm^{-1} peak. The spectra taken with the laser beam parallel to the growth direction had a ratio of 191 cm^{-1} to 211 cm^{-1} peak intensities of 7.1 ± 0.5**,** while this value was consistently lower, at 4.5 ± 0.3, for spectra taken at 90° to the growth direction.

Since the A_g mode (191 cm^{-1} peak) is associated with flexing of the covalently bonded ribbons [12], this anisotropy is crystallographic. Moreover, since the contribution from the A_g mode is greater parallel to the growth direction, and this is consistent with the beam being parallel to the ribbon axis, this implies a growth direction close to [010].

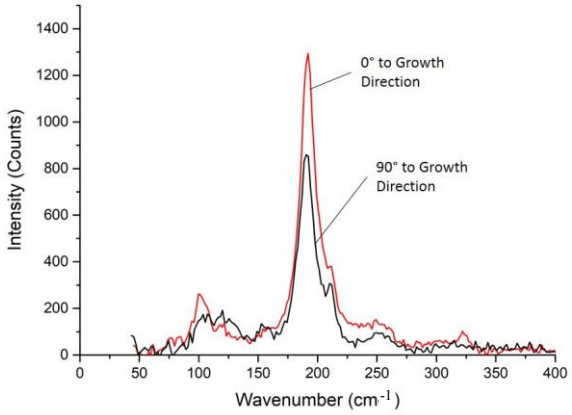

Fig. 6. Typical unpolarized Raman spectra taken at 0° and 90° to the growth direction of a melt-grown single crystal, demonstrating variation in relative intensity of the 191cm^{-1} and 211cm^{-1} peaks.

Raman spectroscopy was also used to confirm the presence of the Sb_2Se_3 phase in static and dynamic vapor-grown crystals, with the 191 cm^{-1} and 211 cm^{-1} peaks being clearly present as in Fig. 6. Moreover, there was no evidence of any Raman signal from the oxide Sb_2O_3 which has a signature at 253 cm^{-1} – growth was therefore confirmed as being oxide-free.

D. Fourier Transform Infrared Spectroscopy

A mm-grained polycrystalline boule produced by dynamic vapor transport was cut into a disk and polished flat for FTIR. The FTIR results shown in Fig. 7 demonstrate a difference in the reflection spectra for s- and p- polarizations. Although the sample used was polycrystalline, this result suggests crystallographic anisotropy, and this would be consistent with Sb_2Se_3 having a preferred growth axis [5]. Moreover, the spectra taken with different polarizations showed some variation, but with notable features at 216, 177, 151, 127 and 90 cm^{-1}. This preliminary work indicates that these samples may be used to identify the IR-active vibrational modes of Sb_2Se_3, with polarization-dependent vibrational modes being predicted by DFT. Use of single crystals would provide a fuller picture of the crystallographic anisotropy.

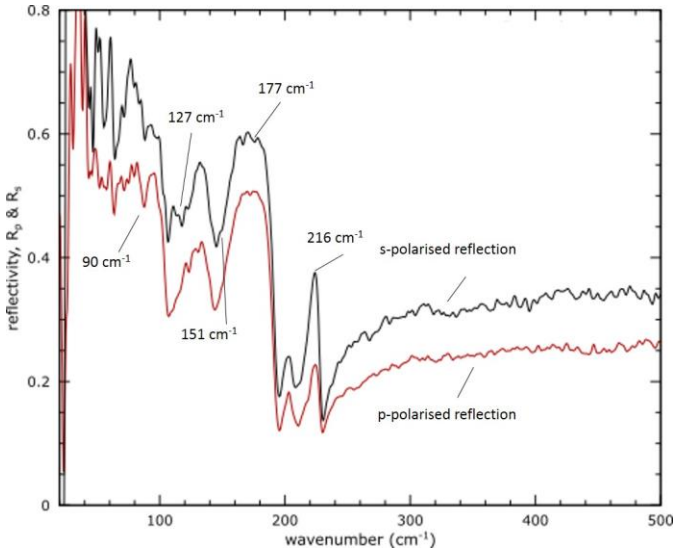

Fig. 7. FTIR reflectivity spectra for s- and p- polarizations, obtained by subtraction of aperture reflectivity and normalization to a gold mirror used as a reflectivity standard. The red and black spectra show the reflectivity of polycrystalline Sb_2Se_3 at different polarizations.

IV. Conclusions

Single crystals of Sb_2Se_3 up to 4 mm in diameter and several cm long were successfully produced by a vertical Bridgman melt-growth method. XRD on these samples offers support to the reported cleavage behavior of Sb_2Se_3 parallel to (100). Both static and dynamic vapor growth methods have been used to form phase-pure polycrystalline boules of Sb_2Se_3, with static vapor growth in particular producing large crystal grain sizes of 0.5 – 2 mm, demonstrating grain growth compared to source powder having particles in the range 1 – 5 μm.

Powder XRD confirmed that the products of the melt- and vapor growth methods were mono-phase orthorhombic, the expected room temperature phase for Sb_2Se_3. Raman spectroscopy of all samples showed strong peaks at 191 and 211 cm^{-1} consistent with literature reports for Sb_2Se_3 thin films and confirmed the absence of oxides. Furthermore, observed changes in the intensity of Raman mode peaks at different orientations of the melt-grown crystals suggested a preference for [010] growth.

These results also highlight the potential for the melt-grown crystals to be used in further fundamental studies. For example, a complete study of the Raman- and IR-active modes with different orientations of the material should be undertaken. The melt-grown crystals are large enough to be mounted for characterization with Hall and Seebeck Effect

measurements, to examine anisotropic behaviors in charge carrier dynamics that are expected from theory. They also offer the possibility of photoluminescence spectroscopy and deep-level-transient spectrometry to examine defects and trap states exclusively present in the bulk. Furthermore, since Sb_2Se_3 has been suggested as a material for which grain boundaries have low recombination velocities [5], the polycrystalline vapor-grown samples could be employed in a quantitative cathodoluminescence investigation. All of these measurements would then provide crucial information on how to optimize the performance of Sb_2Se_3 thin-film photovoltaic devices.

ACKNOWLEDGEMENT

This research was made possible by EPSRC grant EP/M024768/1. TDCH thanks Philip Murgatroyd for providing invaluable advice and technical assistance and also Jonathan Alaria, Jon Major, Dmitry Shchukin for their help.

REFERENCES

[1] K. Zeng, D. J. Xue, and J. Tang, "Antimony selenide thin-film solar cells," *Semicond. Sci. Technol.*, vol. 31, pp. 1–13, 2016.

[2] C. Chen, L. Wang, L. Gao, D. Nam, D. Li, K. Li, Y. Zhao and C. Ge, "6.5% certified efficiency Sb_2Se_3 solar cells using PbS colloidal quantum dot film as hole-transporting layer," *ACS Energy Lett.*, vol. 2, pp. 2125–2132, 2017.

[3] L. J. Phillips, C. N. Savory, P. J. Yates, H. Shiel, O. S. Hutter and M. Birkett, "A scaleable synthesis approach to antimony selenide solar cells," *Submitt. to Nat. Commun.*, 2018.

[4] O. S. Hutter, L. J. Phillips, K. Durose, and J. D. Major, "6.6% efficient antimony selenide solar cells using grain structure control and an organic contact layer," *Submitt. to Sol. Energy Mater. Sol. Cells*, 2018.

[5] Y. Zhou, L. Wang, S. Chen, S. Qin, X. Liu, J. Chen, D. J. Xue, M. Luo, Y. Cao, Y. Cheng, E. H. Sargent and J. Tang, "Thin-film Sb_2Se_3 photovoltaics with oriented one-dimensional ribbons and benign grain boundaries," *Nat. Photonics*, vol. 9, no. 6, pp. 409–415, 2015.

[6] J. J. Carey, J. P. Allen, D. O. Scanlon, and G. W. Watson, "The electronic structure of the antimony chalcogenide series: Prospects for optoelectronic applications," *J. Solid State Chem.*, vol. 213, pp. 116–125, 2014.

[7] R. Vadapoo, S. Krishnan, H. Yilmaz, and C. Marin, "Electronic structure of antimony selenide (Sb_2Se_3) from GW calculations," *Phys. Status Solidi Basic Res.*, vol. 248, no. 3, pp. 700–705, 2011.

[8] R. Caracas and X. Gonze, "First-principles study of the electronic properties of A_2B_3 minerals, with A = Bi, Sb and B = S, Se," *Phys. Chem. Miner.*, vol. 32, pp. 295–300, 2005.

[9] F. Kosek, J. Tulka, and L. Stovrac, "Optical, photoelectric and electric properties of single-crystalline Sb_2Se_3," *Czech J. Phys. B*, vol. 28, pp. 325–330, 1978.

[10] G. Ghosh, "The Sb-Se (antimony-selenium) system," *J. Phase Equilibria*, vol. 14, no. 6, pp. 753–754, 1993.

[11] A. Szczerbakow and K. Durose, "Self-selecting vapour growth of bulk crystals - Principles and applicability," *Prog. Cryst. Growth Characterisation Mater.*, vol. 51, pp. 81–108, 2005.

[12] H. Song, T. Li, J. Zhang, Y. Zhou, J. Luo, C. Chen, B. Yang, C. Ge, Y. Wu and J. Tang, "Highly anisotropic Sb_2Se_3 nanosheets: gentle exfoliation from the bulk precursors possessing 1D crystal structure," *Adv. Mater.*, vol. 29, no. 29, pp. 1–7, 2017.